https://doi.org/10.5194/egusphere-2022-486
Preprint. Discussion started: 4 July 2022

Impacts of urbanization on air quality and related health risks in a city with complex terrain

Chenchao Zhan [a], Min Xie [a,*], Hua Lu [b], Bojun Liu [c], Zheng Wu [b], Tijian Wang [a], Bingliang Zhuang [a], Mengmeng Li [a], Shu Li [a]

[a] School of Atmospheric Sciences, Nanjing University, Nanjing 210023, China

[b] Chongqing Institute of Meteorological Sciences, Chongqing 401147, China

[c] Chongqing Meteorological Observatory, Chongqing 401147, China

---

[*] Corresponding author. minxie@nju.edu.cn (M. Xie)

Abstract: Urbanization affects air pollutants by urban expansion and emission growth, and thereby inevitably changes health risks of air pollutants. However, the health risks related to urbanization are rarely estimated, especially for cities with complex terrain. In this study, a highly urbanized city with severe air pollution and complex terrain (Chengdu) is selected to explore this issue. The effects of urban expansion are further compared with emission growth as air quality management is mainly to regulate emissions. Air pollution in Chengdu is mainly caused by $PM_{2.5}$ and O_3. $PM_{2.5}$ pollution tends to appear in cold months (November to February) due to the secondary circulation forced by complex terrain and the frequent temperature inversion, while O_3 pollution is likely to occur in warm months (April to August) because of high temperature and strong sunlight dominated by high-pressure systems. From 2015 to 2021, the annual total premature mortalities from all non-accidental causes (ANAC) attributed to $PM_{2.5}$ and O_3 exposure are 9386 and 7743, respectively. Based on the characteristics of $PM_{2.5}$ and O_3, six numerical experiments are conducted to investigate the impacts of urban expansion and emission growth on health risks. The results show that urban expansion causes an increase in air temperature and the boundary layer height, which is conducive to the diffusion of $PM_{2.5}$. Thus, surface $PM_{2.5}$ concentrations decrease by 11.7 μg m^{-3} in January. However, the MDA8 O_3 concentrations increase by 10.6 μg m^{-3} in July due to the stronger photochemical production and better vertical mixing during the daytime. Correspondingly, the total premature mortalities from ANAC attributed to $PM_{2.5}$ exposure decrease by 182 (6.9%) in January, but those attributed to O_3 exposure increase by 203 (9.5%) in July. As for the effects of emission growth,

https://doi.org/10.5194/egusphere-2022-486
Preprint. Discussion started: 4 July 2022

$PM_{2.5}$ and MDA8 O_3 concentrations can increase by 26.6 μg m^{-3} and 4.8 μg m^{-3} when anthropogenic emissions are taken into account. The total premature mortalities from ANAC attributed to $PM_{2.5}$ and O_3 exposure then increase by 424 (16.0%) and 87 (4.1%), respectively. The effect of urban expansion on health risks of $PM_{2.5}$ is about half that of anthropogenic emissions. Whereas the effect of urban expansion on health risks of O_3 can be 2.3 times that of anthropogenic emissions. This reminds us that the development of cities is also important for the urban air quality apart from the emissions reduction.

Key Words: urbanization; land use; anthropogenic emissions; air quality; health risk;

1 Introduction

Air pollutants are substances that damage humans, plants and animals drastically when present in the atmosphere in sufficient concentration (Baklanov et al., 2016; Kinney, 2018; Pautasso et al., 2010). The most common air pollutants found in air are ozone (O_3), fine particulate matter ($PM_{2.5}$, particulate matter with an aerodynamic diameter of 2.5 μm or less), sulfur dioxide (SO_2) and nitrogen oxides (NO_x, which is NO + NO_2). These air pollutants threaten human health in many parts of the world, evoking a series of health risks including cardiovascular diseases, respiratory diseases and chronic obstructive pulmonary disease (Brauer et al., 2016; Lelieveld et al., 2013; Manisalidis et al., 2020). According to the World Health Organization (WHO), exposure to ambient air pollutants results in about 4.2 million premature deaths globally per year (https://www.who.int/health-topics/air-pollution#tab=tab_2).

Most of those premature deaths occur in urban areas as urban areas currently host more than 50% of the population (over 3.5 billion people) and this number is projected to increase to 70% by 2050 (UNDESA, 2018). What's more, urban areas are centers of resource utilization and are a major contributor to air pollutant and greenhouse gas emissions. Urbanization, along with socioeconomic development, also leads to increase in anthropogenic emissions. Air pollutants that originate from anthropogenic sources can sometimes accumulate and degrade urban air quality, which leaves urban dwellers vulnerable to air pollution (Holman et al., 2015; Lin and Zhu, 2018). Excessive emissions are considered to be the root cause of poor air quality in urban areas, and thereby efforts have been made to reduce anthropogenic emissions to achieve the goal of managing urban air pollution.

https://doi.org/10.5194/egusphere-2022-486
Preprint. Discussion started: 4 July 2022

In addition to emissions, urban air quality is also closely related to meteorology (Qian et al., 2017). Under calm conditions, local circulations induced by the thermal contrast of the topography, such as mountain-valley breezes and sea-land breezes, are likely to form and play an important role in urban environment (Crosman and Horel, 2010; Zhan and Xie, 2022). Because of historical, political and economic reasons, about 12% of the population (over 720 million people) resides in mountainous areas where air pollution is usually more severe than flat locations since mountainous terrain strongly alters the boundary layer structure, resulting in much more complicated diffusion conditions (Chow et al., 2013). Many notably pollution episodes appear in valley bottoms, along mountain slopes and in mountain basins. These include examples like Mexico City (Molina et al., 2010), Hong Kong (Guo et al., 2013), the Seoul (Ryu et al., 2013), the Salt Lake Valley (Baasandorj et al., 2017), the Colorado Front Range (Bahreini et al., 2018), the Alps (Karl et al., 2019) and the Taiwan Island (Lee et al., 2019). Although the principles behind these examples apply to mountainous areas around the world, the phenomenon being described depends on the particular region (Whiteman, 2000; Oke et al., 2017). And a common principle is that diurnal wind systems driven by mountainous terrain can recirculate urban air pollutants and worsen air quality.

The world has been undergoing urbanization since the industrial revolution in the 19th century (Seto et al., 2012), which directly leads to changes in land use via urban expansion. Natural surfaces are replaced by impervious surfaces, then land surface physical properties (e.g., albedo, thermal inertia and roughness) and processes (e.g., the exchange of water, momentum and energy) are modified, hence altering the urban meteorology and air quality. This has been widely investigated using numerical models. For example, Liao et al. (2015) reported that urban expansion can cause an increase in 2-m temperature by 0.9–2.3 ℃, a decrease in 10-m wind speed by 0.6–1.2 m s^{-1} and an increase in planetary boundary layer height by 100–425 m in the Yangtze River Delta. These changes in meteorology further reduce surface PM_{10} concentrations by 15.3–57.6 μg m^{-3} but increase O_3 concentrations by 1.7–8.3 ppbv. Changes in concentrations of air pollutants inevitably affect their health risks. However, the health risks related to urbanization are rarely estimated, especially for those cities with complex terrain. This is of great concern to policymakers and can inspire future air quality control strategies in mountainous areas.

Chengdu (104.01°E, 30.70°N) is the largest city in western China, occupying an area of 12,390 square kilometers with a population of more than 20 million. Chengdu has the most complex terrain

https://doi.org/10.5194/egusphere-2022-486
Preprint. Discussion started: 4 July 2022

in the world. Located in the west of the Sichuan Basin, this city is surrounded by the Tibetan Plateau to the west, the Wu Mountains to the east, the Yunnan-Guizhou Plateau to the south and the Daba Mountains to the north (Figure 1a). In addition, the urbanization of Chengdu has developed rapidly over the past few decades (Dai et al., 2021). The fast urbanization process is generally accompanied by a surge in urban construction lands and the loss of cropland (Figure 1c). Luo et al. (2021) reported that Chengdu's urban area has increased by four times from 1996 to 2016. Due to substantial emissions from human activities (Figure 1b) and poor atmospheric diffusion capacity caused by complex terrain, Chengdu is one of the most polluted cities in China and has suffered from severe $PM_{2.5}$ and O_3 pollution in recent years (Shu et al., 2021; Yang et al., 2020; Zhan et al., 2019). Complex terrain, rapid urbanization and severe air pollution make Chengdu an ideal place to study the impact of urbanization on health risks of air pollutants in mountainous areas.

In this study, we systematically evaluate the impacts of urbanization on air quality and the corresponding health risks in Chengdu. We also compare the impacts of urban expansion with emission growth. First, the basic characteristics of air pollutants in Chengdu from 2015 to 2021 are illustrated. Then, the impacts of urbanization on air pollutants are investigated by using the WRF-Chem model. Finally, premature mortalities attributed to changes in air pollutants are estimated by using the standard damage function. The rest of this paper is organized as follows. Section 2 introduces the observation data, the model configurations and the experimental designs. Section 3 shows the main results and discussions. The conclusions are given in Section 4.

https://doi.org/10.5194/egusphere-2022-486
Preprint. Discussion started: 4 July 2022

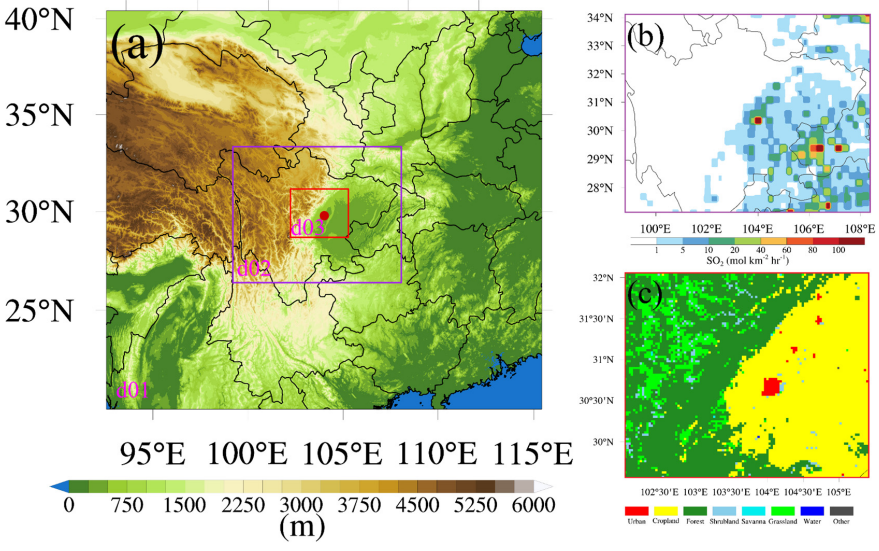

Figure 1. Three nested WRF-Chem domains, including (a) domain 1 with terrain heights, (b) domain 2 with SO_2 emissions and (c) domain 3 with land cover maps. The red dot in (a) shows the location of Chengdu.

2 Materials and methods

2.1 Air pollutants and meteorological data

Air pollutants, including $PM_{2.5}$, PM_{10}, O_3, NO_2, SO_2 and CO, are monitored by the National Environmental Monitoring Center (NEMC) of China. These data are hourly issued on the national urban air quality real-time publishing platform (http://106.37.208.233:20035/). This nationwide observation network consists of more than 2300 stations distributed over 450 cities in China.

Surface meteorological data, including 2-m air temperature (T_2), relative humidity (RH) and 10-m wind speed (WS_{10}) and direction (WD_{10}), are taken from the website of the University of Wyoming (http://weather.uwyo.edu/surface/). To verify upper-air fields, the sounding observations at Wenjiang (103.87°E, 30.75°N) in Chengdu are also acquired from this website. These sounding data contain temperature, relative humidity and wind speed etc. at different pressure layers with a time resolution of 12 h (00:00 and 12:00 UTC), and are often plotted on a Skew-T diagram (https://www.ncl.ucar.edu/Applications/skewt.shtml#ex2).

In this study, the data quality control are performed as follows. First, the data indicated as

https://doi.org/10.5194/egusphere-2022-486
Preprint. Discussion started: 4 July 2022

missing are set as invalid. Second, the urban values are calculated by averaging observations at all monitoring sites in Chengdu. Third, the daily maximum 8 h average (MDA8) O_3 concentrations are calculated only on days with more than 18 h of O_3 concentrations measurements.

2.2 WRF-Chem model and experimental designs

WRF-Chem is the Weather Research and Forecasting (WRF) model coupled with Chemistry, in which meteorological and chemical variables use the same coordinates, transport schemes and physics schemes in space and time (Grell et al., 2005). WRF-Chem version 3.9.1 is employed in this study. As shown in Figure 1a, three nested domains are used with the grid spacing of 27, 9 and 3 km, respectively. 32 sigma levels are extending from the surface to 100 hPa in the vertical direction with 12 levels located below 2 km to resolve the boundary layer processes. The MODIS-based land use data set as default in WRF are selected. The domains and main options for physical and chemical parameterization schemes are listed in Table 1. The National Centers for Environmental Prediction (NCEP) global final analysis data with a horizontal resolution of 1° × 1° at 6 h time intervals are adopted as the initial and boundary conditions. Anthropogenic emissions are provided by the Multi-resolution Emission Inventory for China (MEIC) in 2017 at 0.25° × 0.25° resolution. Biogenic emissions are calculated online using the Guenther scheme (Guenther et al., 2006).

Table 1. The domains and main options for WRF-Chem.

Items	Contents
Domains (x, y)	(94, 86), (109, 88), (112, 94)
Grid spacing (km)	27, 9, 3
Center	(104°E, 31°N)
Time step (s)	90
Microphysics	Purdue Lin scheme (Chen and Sun, 2002)
Longwave radiation	RRTM scheme (Mlawer et al., 1997)
Shortwave radiation	Goddard shortwave scheme (Matsui et al., 2018)
Surface layer	Monin-Obukhov scheme (Janjic, 1994)
Land-surface layer	Unified Noah land-surface model (Tewari et al., 2014)
Planetary boundary layer	Mellor-Yamada-Janjic TKE scheme (Janjic, 1994)

https://doi.org/10.5194/egusphere-2022-486
Preprint. Discussion started: 4 July 2022

Cumulus parameterization	Grell 3D ensemble scheme (Grell and Devenyi, 2002)
Gas-phase chemistry	RADM2 (Stockwell et al., 1990)
Photolysis scheme	Fast-J photolysis (Fast et al., 2006)
Aerosol module	MADE/SORGAM (Schell et al., 2001)

To investigate the impacts of urban expansion and anthropogenic emissions, six numerical experiments are designed (Table 2). The year of the numerical simulations is 2017 since the anthropogenic emissions are currently updated to 2017. Moreover, January is representative of the cold months with frequent $PM_{2.5}$ pollution, while July represents the hot season with frequent O_3 pollution (Section 3.1). Jan_Base simulation is a baseline simulation using the MODIS land use and the MEIC anthropogenic emission inventory over all three domains. SO_2 emissions in domain 2 and land cover maps in domain 3 are illustrated in Figure 1b and 1c. Jan_noCD is a sensitivity simulation, in which the urban land surface of Chengdu is replaced by cropland to examine the impacts of urban expansion. Jan_noEmi is also a sensitivity simulation, in which the anthropogenic emissions in Chengdu are shut down to identify the impacts of anthropogenic emissions. The above three numerical experiments used the same configurations (Table 1) running from 00:00 UTC December 28, 2016 to 00:00 UTC February 1, 2017 with the first 96 h as spin-up time. July_Base, July_noCD and July_noEmi are the same as Jan_Base, Jan_noCD and Jan_noEmi, but run from 00:00 UTC June 27 to 00:00 UTC August 1, 2017 with the first 96 h as spin-up time.

Table 2. Six numerical experiments are conducted in this study.

Scenarios	Description
Jan_Base	Baseline simulation in January
Jan_noCD	Replacing urban land use of Chengdu with cropland in January
Jan_noEmi	Shutting down anthropogenic emissions in Chengdu in January
July_Base	Baseline simulation in July
July_noCD	Replacing urban land use of Chengdu with cropland in July
July_noEmi	Shutting down anthropogenic emissions in Chengdu in July

https://doi.org/10.5194/egusphere-2022-486
Preprint. Discussion started: 4 July 2022

2.3 Health risks estimation

Daily premature mortalities attributed to $PM_{2.5}$ and O_3 exposure from all non-accidental causes (ANAC), cardiovascular diseases (CVD), respiratory diseases (RD) and chronic obstructive pulmonary diseases (COPD) are estimated using the standard damage function (Anenberg et al., 2010; Zhan et al., 2021):

$$\Delta M = y_0(\frac{RR-1}{RR})\mathrm{Pop}, \quad (4)$$

where ΔM is the daily premature mortality, y_0 is the daily baseline mortality rate, RR is the relative risk, $(RR-1)/RR$ is the attributable fraction, and Pop is the exposed population. RR is calculated as follows:

$$RR = \exp(\beta(\mathrm{C}-\mathrm{C}_0)), \quad (5)$$

where β is the concentration-response function, which represents the percentage increase in health effect per 1 μg m^{-3} $PM_{2.5}$ and MDA8 O_3 increment. C is the exposure concentration, and C_0 is the threshold concentration.

In this study, C_0 for $PM_{2.5}$ is 10 μg m^{-3} (Song et al., 2015), and for MDA8 O_3 is 75.2 μg m^{-3} (Liu et al., 2018). The β and y_0 values for ANAC, CVD, RD and COPD are summarized in Table 3 (Chen et al., 2017; Yin et al., 2017). The populations of Chengdu provided by the National Bureau of Statistics of China are 16.853 million, 18.582 million, 19.188 million, 19.183 million, 20.409 million, 20.947 million and 20.938 million from 2015 to 2021.

Table 3. Daily β and y_0 values for ANAC, CVD, RD and COPD. This table is cited from Wang et al. (2021).

Disease	β for $PM_{2.5}$ (%)	β for MDA8 O_3 (%)	y_0
ANAC	0.22	0.24	1.687×10^{-5}
CVD	0.27	0.27	3.880×10^{-6}
RD	0.29	0.18	1.841×10^{-6}
COPD	0.38	0.20	1.623×10^{-6}

3 Results and discussions

3.1 $PM_{2.5}$ and O_3 pollution in Chengdu

https://doi.org/10.5194/egusphere-2022-486
Preprint. Discussion started: 4 July 2022

$PM_{2.5}$ and O_3 are two crucial air pollutants that account for air pollution. The Chinese ambient air quality standards for $PM_{2.5}$ and MDA8 O_3 are 75 μg m^{-3} and 160 μg m^{-3}, respectively. As shown in Figure 2, Chengdu is suffering from severe $PM_{2.5}$ and O_3 pollution in recent years. There are 97, 101, 68, 53, 33, 43 and 37 $PM_{2.5}$ pollution episodes, and 61, 48, 42, 40, 26, 50 and 27 O_3 pollution episodes in Chengdu from 2015 to 2021. The annual average concentrations of $PM_{2.5}$ are 60.7, 59.9, 52.6, 47.2, 40.6, 40.8 and 40.1 μg m^{-3}, and those of MDA8 O_3 are 95.3, 96.4, 95.8, 101.3, 86.8, 92.0 and 89.6 μg m^{-3}, respectively. In terms of the annual average concentrations, $PM_{2.5}$ pollution has improved significantly while O_3 pollution has not. In addition, $PM_{2.5}$ and O_3 pollution have clear seasonal preferences, that is, $PM_{2.5}$ pollution tends to appear in cold months (November to February) while O_3 pollution prefers to appear in warm months (April to August). High $PM_{2.5}$ concentrations in cold months may be associated with the consumption of fossil fuels for heating and frequent temperature inversion. Elevated O_3 concentrations in warm months are contributed to the high temperature and strong sunlight.

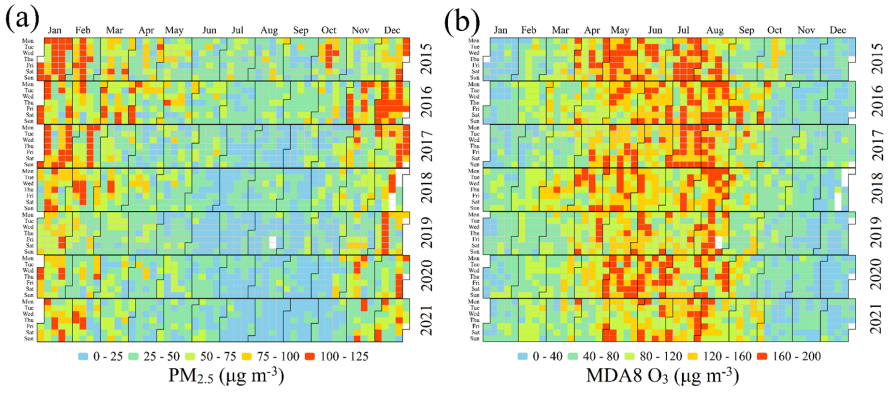

Figure 2. Distribution of (a) daily average $PM_{2.5}$ and (b) MDA8 O_3 concentrations in Chengdu from 2015 to 2021.

3.2 Premature mortality attributed to $PM_{2.5}$ and O_3

Severe $PM_{2.5}$ and O_3 pollution are responsible for a considerable number of premature mortalities in Chengdu. As shown in Table 4, the premature mortalities from ANAC attributed to $PM_{2.5}$ exposure are 10596, 11647, 10154, 8942, 7993, 8298 and 8072 from 2015 to 2021, with an annual average of 9386. The highest health risk among the diseases is from CVD with an annual

https://doi.org/10.5194/egusphere-2022-486
Preprint. Discussion started: 4 July 2022

average of 2609, followed by COPD with an annual average of 1485 and RD with an annual average of 1321. Due to urbanization and administrative division adjustment, Chengdu's population increases by 24.2% from 2015 (16.853 million) to 2021 (20.938 million). In contrast, the total premature mortalities attributed to $PM_{2.5}$ falls by 23.8% from 2015 (10596) to 2021 (8072). The reduction in premature mortalities is mainly contributed to the reduction in $PM_{2.5}$ concentrations since the annual average $PM_{2.5}$ concentrations decrease from 60.7 μg m^{-3} in 2015 to 40.1 μg m^{-3} in 2021 (Section 3.1), suggesting that air pollution control can bring huge health benefits.

Unlike the overall reduction in premature mortalities due to $PM_{2.5}$, the premature mortalities due to O_3 fluctuate. The premature mortalities from ANAC attributed to O_3 exposure are 7657, 8025, 7870, 8556, 6367, 8300 and 7429 from 2015 to 2021, with an annual average of 7743, about 80% of that attributed to $PM_{2.5}$ exposure. The total premature mortalities attributed to O_3 exposure in 2021 (7429) are only 3.0% lower than that in 2015 (7657). This is in line with the insignificant reduction of O_3 concentrations in Chengdu from 2015 to 2021, indicating that O_3 pollution control in Chengdu still has great potential and significance.

Table 4. Premature mortality from ANAC, CVD, RD and COPD attributed to $PM_{2.5}$ and O_3 exposure.

Year	$PM_{2.5}$				MDA8 O_3			
	ANAC	CVD	RD	COPD	ANAC	CVD	RD	COPD
2015	10596	2935	1485	1660	7657	1957	643	624
2016	11647	3231	1635	1832	8025	2053	672	653
2017	10154	2812	1422	1589	7870	2013	659	641
2018	8942	2490	1262	1424	8556	2191	715	696
2019	7993	2230	1131	1280	6367	1630	532	518
2020	8298	2313	1173	1325	8300	2121	696	677
2021	8072	2249	1140	1287	7429	1902	621	604

3.3 Impacts of urbanization on $PM_{2.5}$ and O_3

3.3.1 Meteorological conditions in January and July

In this study, January and July 2017 are chosen for simulations and analysis when $PM_{2.5}$ and

https://doi.org/10.5194/egusphere-2022-486
Preprint. Discussion started: 4 July 2022

O_3 pollution are likely to occur (Figure 2). In January 2017, Chengdu experiences $PM_{2.5}$ pollution for 23 out of 31 days with an average concentration of 128.5 μg m^{-3}. From the perspective of atmospheric circulations, westerly winds prevail over Chengdu due to the large north-south geopotential height gradient at 500 hPa (Figure 3a). However, the cold westerly winds from the north are blocked by the Tibetan Plateau. Instead, a low-pressure system, called the Southwest Vortex, appears to the left of Chengdu at 850 hPa (Figure 3b). Warm and humid southerly air flows can reach Chengdu affected by this low-pressure system (Hu et al., 2021; Ning et al., 2018). The dry air in the upper layer and moist air in the lower layer lead to a strong temperature inversion appearing from 700 hPa to 500 hPa (Figure 4a and b). The blocking of clod air and the temperature inversion make $PM_{2.5}$ pollution frequent during this period.

In July 2017, there are 19 days of O_3 pollution in Chengdu, and the average MDA8 O_3 concentration is 172.9 μg m^{-3}. At 500 hPa, Chengdu is dominated by strong high-pressure systems, and thereby air temperature is high and wind speed is small (Figure 3c). The average T_2 is as high as 28.6 ℃ while the average WS_{10} is only 1.6 m s^{-1} in July. These meteorological conditions are conducive to the formation of O_3 pollution. Furthermore, the frequency and thickness of temperature inversion in July are far less than those in January (Figure 4). Then O_3 can be well mixed within the mixing layer during the daytime, which is an important way to maintain high surface O_3 concentrations (Aneja et al., 2000; Tang et al., 2017).

https://doi.org/10.5194/egusphere-2022-486
Preprint. Discussion started: 4 July 2022

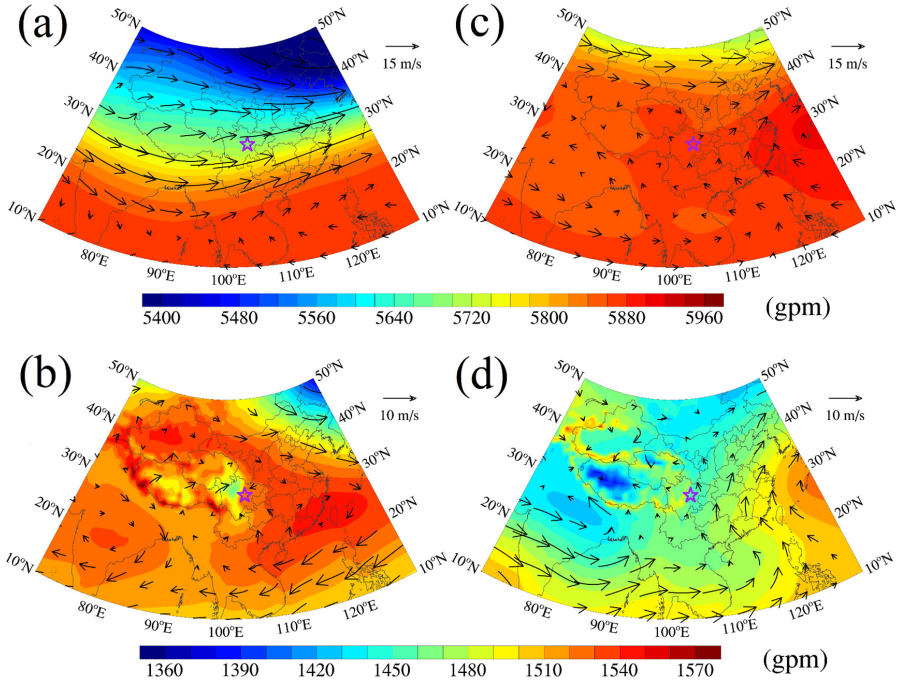

Figure 3. The weather charts at (a) 500 hPa and (b) 850 hPa for January 2017. (c) and (d) are the same as (a) and (b), but for July 2017. The purple pentacles show the location of Chengdu. These weather charts are based on the NCEP global final analysis data.

https://doi.org/10.5194/egusphere-2022-486
Preprint. Discussion started: 4 July 2022

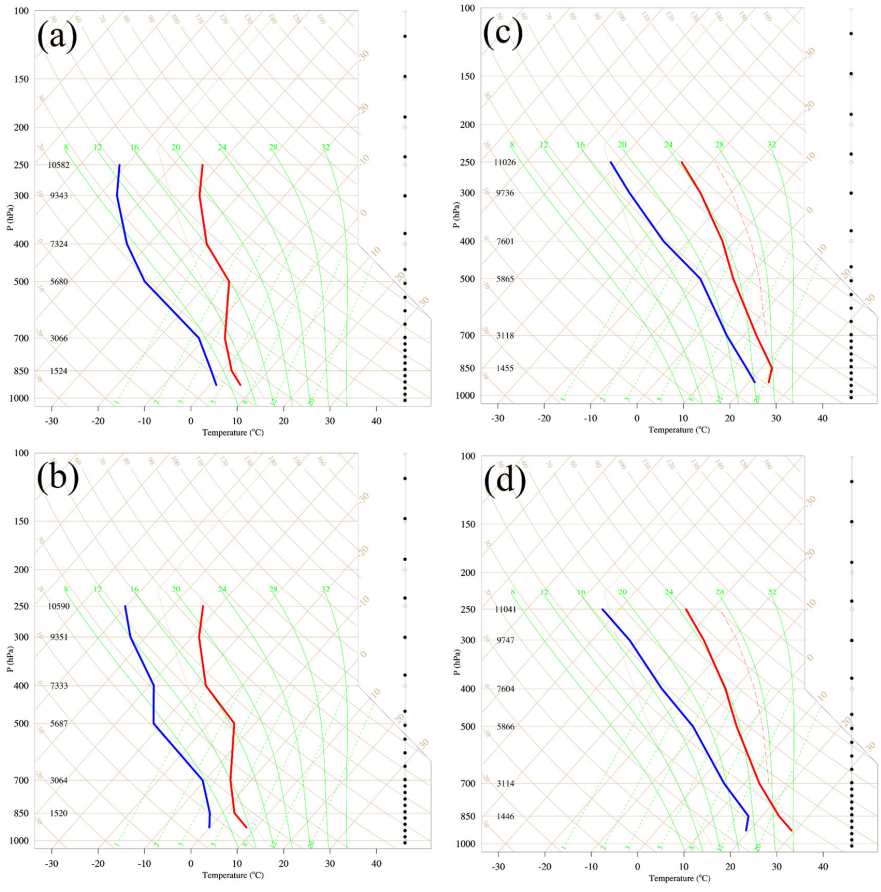

Figure 4. The skew-T diagram at (a) 00:00 UTC and (b) 12:00 UTC in January 2017. (c) and (d) are the same as (a) and (b), but for July 2017. The red and blue lines indicate air temperature and dew point temperature, respectively.

3.3.2 Evaluation of model performance

Simulated $PM_{2.5}$ concentrations, O_3 concentrations, air temperature, relative humidity and wind speed in baseline simulations are compared with the observations to verify the model performance (Figure 5). The magnitudes of simulated $PM_{2.5}$ and O_3 are reasonable with the small mean bias (MB) of 23.4 and 11.6 μg m^{-3}, respectively. The high correlation coefficients (COR) for $PM_{2.5}$ (0.44) and O_3 (0.77) indicate that simulations reproduce well the diurnal variation in pollutants. Therefore, the modeling results for $PM_{2.5}$ and O_3 are generally reasonable and acceptable. With regard to the meteorological factors, T_2 is well simulated with low MB (0.2 and 0.1 ℃) and

https://doi.org/10.5194/egusphere-2022-486
Preprint. Discussion started: 4 July 2022

high COR (0.76 and 0.70) values in both January and July. Our simulation underestimates RH to some extent (the MB values are -14.3% and -4.8% in January and July, respectively), but the diurnal variation of RH is well represented (the COR values are 0.54 and 0.64). As for WS_{10}, poor simulation results are predictable in the case of low wind and complex terrain. The WS_{10} in the model is overestimated (the MB values are 1.3 and 1.7 m s^{-1}), which may be related to the unresolved terrain features by the default surface drag parameterization causing an overestimate of wind speed in particular at low values (Jimenez and Dudhia, 2012). Due to the small change in weak wind, the COR for WS_{10} is not high. In general, the WRF-Chem model using our configuration has a good capability in simulating air pollutants and meteorological factors in Chengdu, and thereby the simulations can be used for subsequent analysis.

https://doi.org/10.5194/egusphere-2022-486
Preprint. Discussion started: 4 July 2022

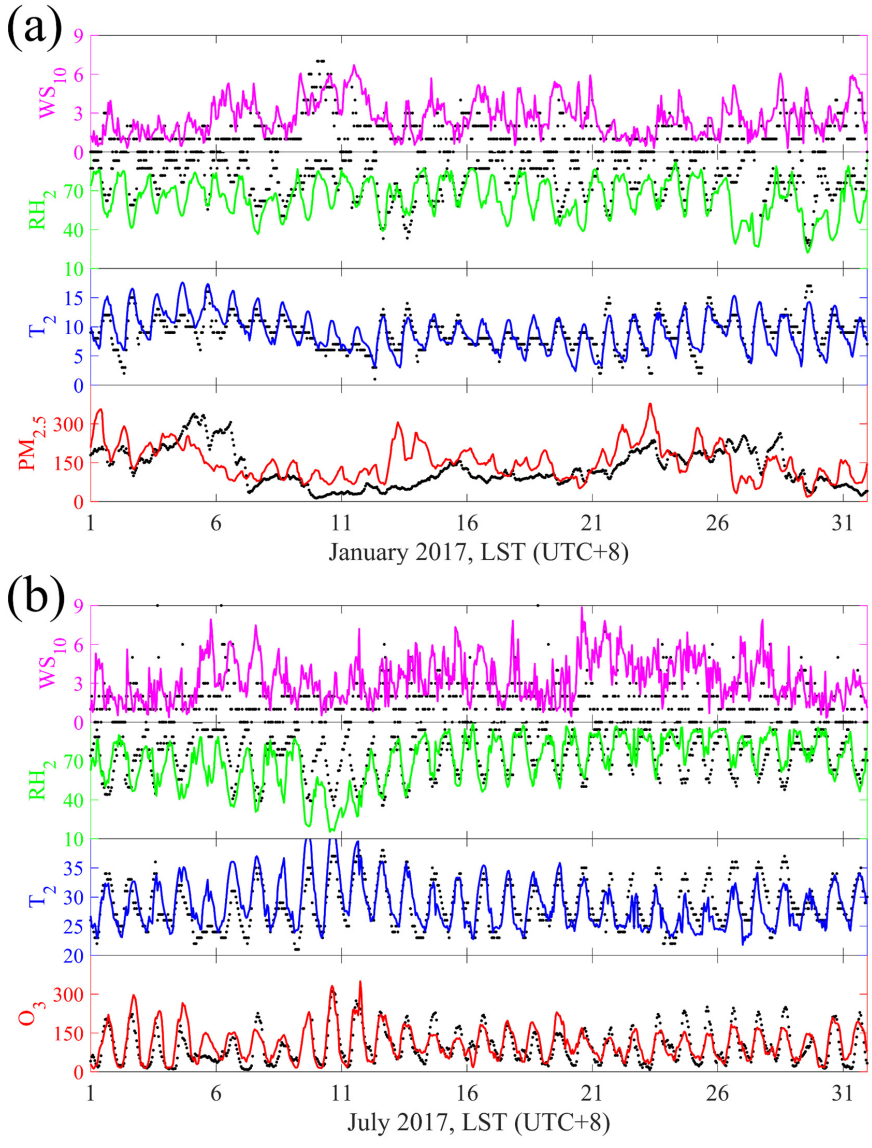

Figure 5. Times series of $PM_{2.5}$, O_3, T_2, RH and WS_{10} for observations (black dots) and baseline simulations (colored lines).

3.3.3 Spatiotemporal variations in $PM_{2.5}$ and O_3

Figure 6 shows the January-averaged spatiotemporal distribution of $PM_{2.5}$ in Jan_Base simulation. $PM_{2.5}$ has a diurnal variation with high concentration at night and low concentration at

https://doi.org/10.5194/egusphere-2022-486
Preprint. Discussion started: 4 July 2022

noon, which is contrary to the diurnal variation of the boundary layer height. At night, the boundary layer height is usually low. As a consequence, $PM_{2.5}$ is trapped and maintained on the ground. At noon, turbulence in the convective boundary layer can dilute $PM_{2.5}$ concentrations through vertical mixing, resulting in low $PM_{2.5}$ concentrations at surface. Chengdu is on the east side of the Tibetan Plateau, with a large elevation drop exceeding 3000 m over a short horizontal distance (Figure 1a). In this case, the mountain-valley breezes can easily develop in winter when atmospheric conditions are usually stagnant, and are crucial for $PM_{2.5}$ in Chengdu. The $PM_{2.5}$ pollution zone tends to appear in the converging airflows associated with the mountain breezes and can spread hundreds of kilometers (Figure 6a-d). Driven by the near-surface northeasterly winds, $PM_{2.5}$ is uplifted over the windward slope of the Tibetan Plateau (Figure 6e-h). Then the uphill airflows are restrained and overturned below 3 km, forming a vertical secondary circulation over Chengdu. Governed by the secondary circulation forced by the complex terrain, the southwesterly winds at 3 km can transport $PM_{2.5}$ downward, which could replenish the surface $PM_{2.5}$ and facilitate the accumulation and maintenance of surface $PM_{2.5}$.

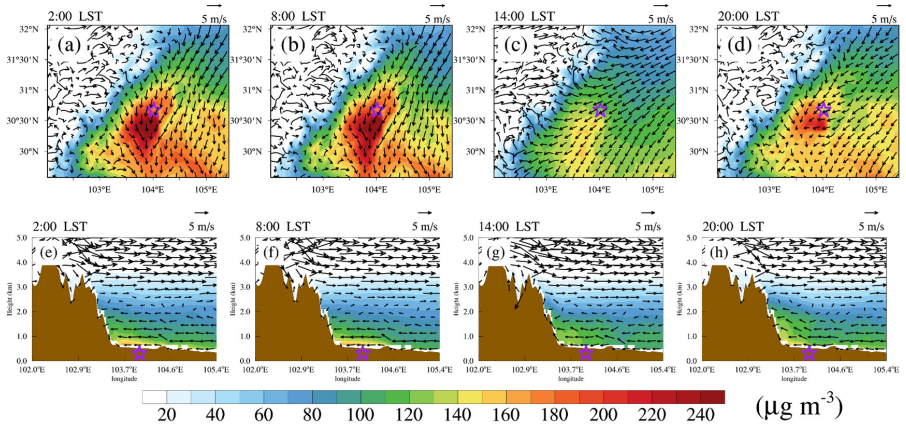

Figure 6. (a-d) Spatial distributions and (e-h) east-west vertical cross sections of $PM_{2.5}$ with wind fields at 2:00, 8:00, 14:00 and 20:00 LST (LST is UTC+8h) in Jan_Base simulation. Purple pentacles show the location of Chengdu. Brown-shaded areas represent the terrain.

In terms of O_3, it exhibits strong diurnal variation with an afternoon maximum and an early

https://doi.org/10.5194/egusphere-2022-486
Preprint. Discussion started: 4 July 2022

morning minimum (Figure 7a-d). After sunrise, the nocturnal residual layer is destroyed while the convective boundary layer begins to form as the surface is heated. This leads to downward mixing of O_3 from aloft (Hu et al., 2018; Zhan and Xie, 2022). Meanwhile, O_3 is also generated by photochemical reactions between volatile organic compounds (VOCs) and NO_x in the presence of sunlight. As a consequence, O_3 concentrations increase rapidly from morning to noon (Figure 7b, 7c, 7f and 7g). By noon, O_3 can be well mixed within the convective boundary layer via strong turbulence. Strong photochemical production and well mixing cause high O_3 concentrations until late afternoon (Figure 7c, 7d, 7g and 7h). Thereafter, O_3 production decreases since the intensity of sunlight diminishes. After sunset, O_3 concentrations decrease substantially due to surface deposition and nitrogen oxide titration ($O_3 + NO \rightarrow O_2 + NO_2$) and reach their minimum in the early morning (Figure 7a, 7d, 7e and 7h). But O_3 in the nocturnal residual layer is still at a high level with values more than 140 μg m^{-3}. Compared with the Jan_Base simulation, the secondary circulation forced by the complex terrain is not obvious. In addition, O_3 with a concentration of about 100 μg m^{-3} has always existed over the Tibetan Plateau, but $PM_{2.5}$ concentrations there are quite low. This indicates that the background concentration of O_3 is much higher than that of $PM_{2.5}$, which may pose a huge challenge to O_3 pollution control.

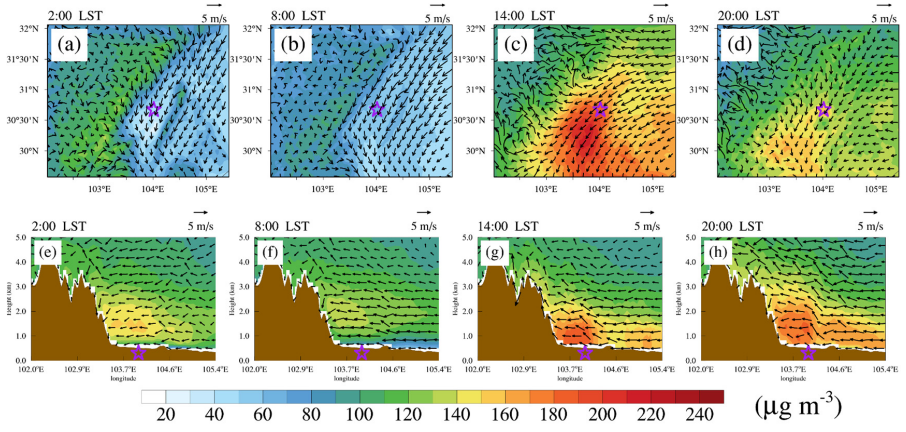

Figure 7. (a-d) Spatial distributions and (e-h) east-west vertical cross sections of O_3 with wind fields at 2:00, 8:00, 14:00 and 20:00 LST (LST is UTC+8h) in July_Base simulation. Purple pentacles show the location of Chengdu. Brown-shaded areas represent the terrain.

https://doi.org/10.5194/egusphere-2022-486
Preprint. Discussion started: 4 July 2022

3.3.4 Impacts of urban expansion on $PM_{2.5}$ and O_3

Modification of urban land use changes surface dynamic and thermal characteristics, and thereby affects the transportation and dispersion of air pollutants. Figure 8 shows the differences in $PM_{2.5}$ between Jan_Base and Jan_noCD simulations (Jan_Base minus Jan_noCD). Results show that surface $PM_{2.5}$ concentrations in Jan_Base simulation are lower at all times compared with Jan_noCD simulation, with the monthly average decreasing by 11.7 μg m^{-3} (Figure 8a-d). Moreover, the decrease in $PM_{2.5}$ is larger during the nighttime than during the daytime. Specially, surface $PM_{2.5}$ concentrations decrease by 15.0 μg m^{-3} at 2:00 LST and 3.2 μg m^{-3} at 14:00 LST. The decrease in surface $PM_{2.5}$ is mainly attributed to the modification of the boundary layer height. Urban land use can enhance surface heating leading to an increase in air temperature, known as the urban heat island. The vertical air movement is then enhanced by the warming up of surface air temperature, resulting in an increase in the boundary layer height, which facilitates the vertical diffusion of surface $PM_{2.5}$. $PM_{2.5}$ concentrations increase by 2-6 μg m^{-3} in the upper boundary layer (~1 km above the surface) (Figure 8e-h), further confirming this point.

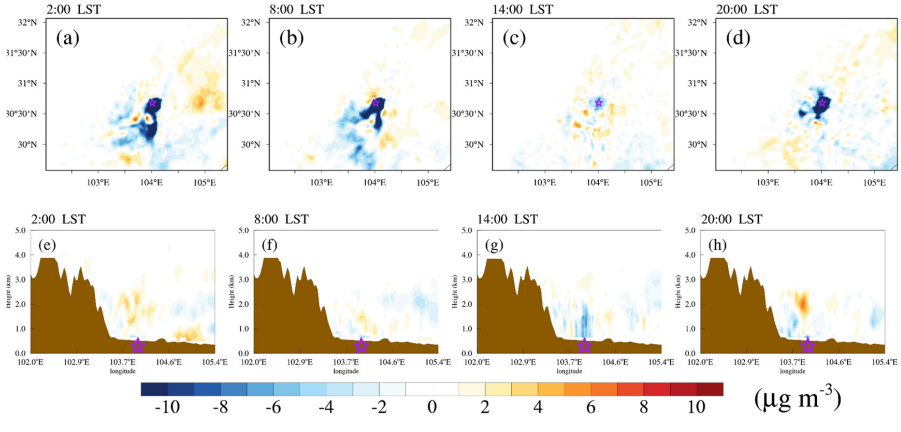

Figure 8. (a-d) Spatial distributions and (e-h) east-west vertical cross sections of the differences in $PM_{2.5}$ between Jan_Base and Jan_noCD simulations (Jan_Base minus Jan_noCD). Purple pentacles show the location of Chengdu. Brown-shaded areas represent the terrain.

https://doi.org/10.5194/egusphere-2022-486
Preprint. Discussion started: 4 July 2022

O_3 is a secondary air pollutant that is not only related to meteorological conditions but also to its precursors (VOCs and NO_x). Due to the increase in upward air movement and boundary layer height induced by urban land use, $PM_{2.5}$ and NO_x concentrations decrease near the surface but increase in the upper boundary layer (Liao et al., 2015; Zhu et al., 2017). The decrease in NO_x near the surface results in an increase in surface O_3 at night since the NO_x titration is weakened (Figure 9a and d). Although the elevated boundary layer dilutes O_3 concentrations to some extent, the nighttime O_3 concentrations are mainly dominated by chemical effects and eventually increase by a maximum of 25.8 μg m^{-3}. During the daytime, the increased air temperature is conducive to the photochemical production of O_3, and the well-developed convective boundary layer favors vertical mixing of O_3. O_3 concentrations will also increase (Figure 9b and c), with the value of 4.4 μg m^{-3} at 14:00 LST in Chengdu. Finally, MDA8 O_3 concentrations in July can increase by 10.6 μg m^{-3} due to the effects of urban expansion.

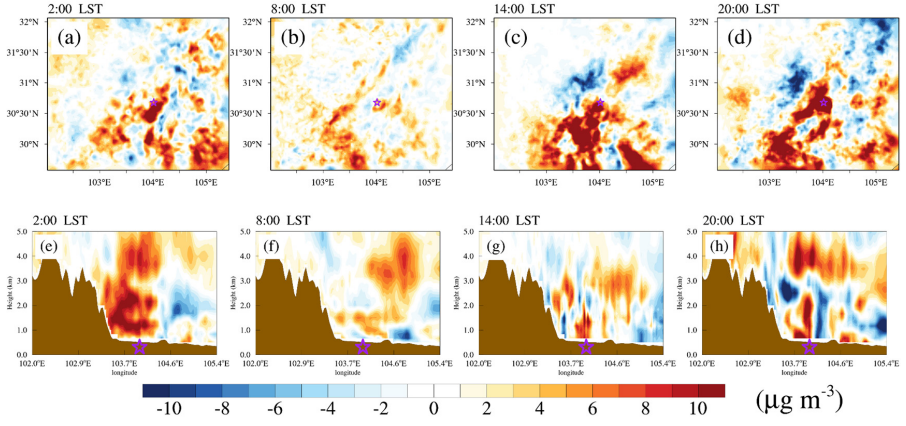

Figure 9. (a-d) Spatial distributions and (e-h) east-west vertical cross sections of the differences in O_3 between July_Base and July_noCD simulations (July_Base minus July_noCD). Purple pentacles show the location of Chengdu. Brown-shaded areas represent the terrain.

3.3.5 Impacts of anthropogenic emissions on $PM_{2.5}$ and O_3

Air pollutants become part of the air once released, and they do not have a direct effect on airflows like temperature or radiation. Therefore, the impacts of anthropogenic emissions are more

https://doi.org/10.5194/egusphere-2022-486
Preprint. Discussion started: 4 July 2022

intuitive than urban expansion. Figure 10 shows the differences in $PM_{2.5}$ between Jan_Base and Jan_noEmi simulations (Jan_Base minus Jan_noEmi). $PM_{2.5}$ concentrations in Jan_Base simulation are significantly higher than those in Jan_noEmi simulations, with the monthly average concentration increasing by 26.6 μg m^{-3}, more than twice the difference between Jan_Base and Jan_noCD simulations. Furthermore, the increase in $PM_{2.5}$ appears throughout the boundary layer (Figure 10e-h) and can extend downstream for hundreds of kilometers (Figure 10a-d), indicating that reducing anthropogenic emissions is an effective way to reduce $PM_{2.5}$ concentrations.

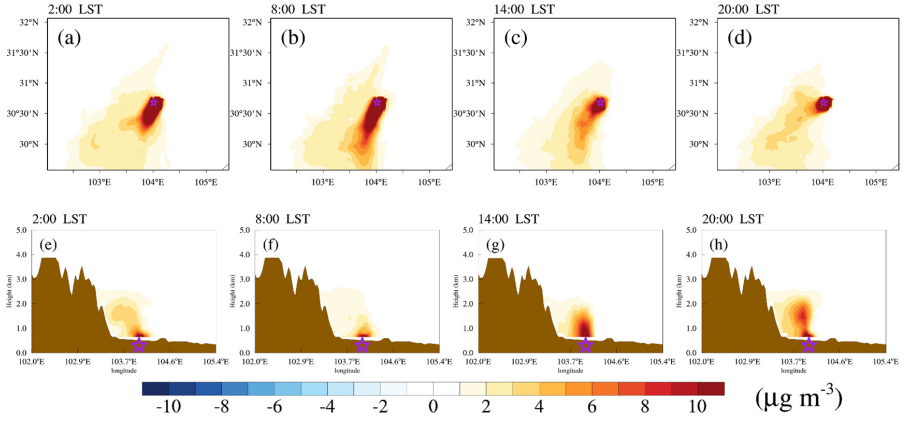

Figure 10. (a-d) Spatial distributions and (e-h) east-west vertical cross sections of the differences in $PM_{2.5}$ between Jan_Base and Jan_noEmi simulations (Jan_Base minus Jan_noEmi). Purple pentacles show the location of Chengdu. Brown-shaded areas represent the terrain.

As for O_3, O_3 concentrations in July_Base simulation are 5.8 μg m^{-3} higher than those in July_noEmis simulation at 14:00 LST due to the abundance of O_3 precursors (Figure 11c). However, O_3 concentrations decrease by 3.4 μg m^{-3} at 2:00 LST (Figure 11a). This phenomenon may be related to the non-linear sensitivity of O_3 to VOCs and NO_x precursor emissions. O_3 formation regimes are often classified into VOC-limited, NO_x-limited and transition regimes depending on the ratio of VOCs and NO_x (Jin et al., 2020; Lu et al., 2019). At low VOC/NO_x ratios (VOC-limited regime, usually in urban areas), reducing the concentrations of NO_x would lead to an increase in O_3

https://doi.org/10.5194/egusphere-2022-486
Preprint. Discussion started: 4 July 2022

formation. Apart from the amount of anthropogenic emissions, a reasonable emission reduction path is also necessary to alleviate O_3 pollution. Since O_3 concentrations increase during the daytime, MDA8 O_3 concentrations in July_Base simulation are still 4.8 μg m^{-3} higher than those in July_noEmis simulation.

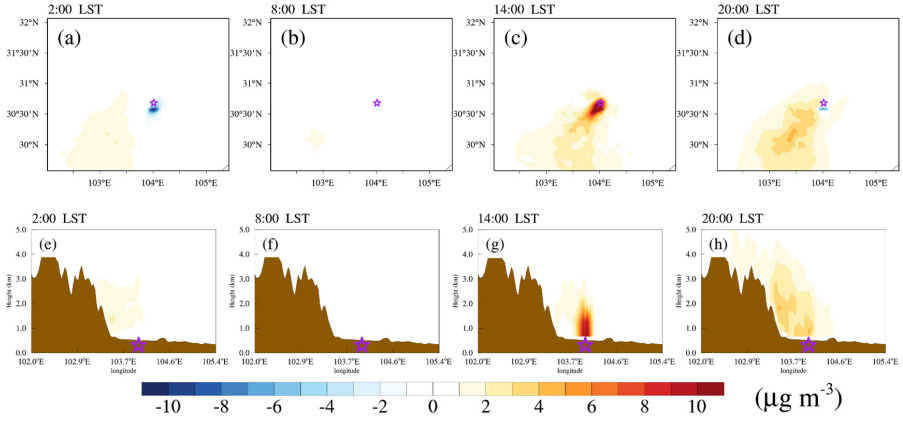

Figure 11. (a-d) Spatial distributions and (e-h) east-west vertical cross sections of the differences in O_3 between July_Base and July_noEmi simulations (July_Base minus July_noEmi). Purple pentacles show the location of Chengdu. Brown-shaded areas represent the terrain.

3.4 Health risks caused by urbanization

According to the above results, urban expansion can decrease surface $PM_{2.5}$ by 11.7 μg m^{-3} but increase MDA8 O_3 by 10.6 μg m^{-3}. On the other hand, anthropogenic emissions can increase surface $PM_{2.5}$ by 26.6 μg m^{-3} and MDA8 O_3 by 4.8 μg m^{-3}. We then calculate the premature mortalities under different simulation scenarios to access the health risks from changes in $PM_{2.5}$ and O_3 concentrations. As shown in Figure 12, the premature mortalities from ANAC, CVD, RD and COPD due to $PM_{2.5}$ decrease by 182 (6.9%), 47 (6.5%), 23 (6.4%) and 24 (6.1%) in January 2017 with the existence of Chengdu. While anthropogenic emissions in Chengdu increase premature mortalities from ANAC, CVD, RD and COPD due to $PM_{2.5}$ by 424 (16.0%), 111 (15.4%), 55 (15.2%) and 56 (14.3%), respectively. With regard to O_3, premature mortalities from the O_3-induced diseases all

https://doi.org/10.5194/egusphere-2022-486
Preprint. Discussion started: 4 July 2022

increase when urban land use and anthropogenic emissions are taken into account. Urban expansion leads to an increase of premature mortalities from ANAC, CVD, RD and COPD due to O_3 by 203 (9.5%), 51 (9.4%), 18 (10.0%) and 17 (9.7%) in July 2017, respectively. When anthropogenic emissions in Chengdu are turned on, premature mortalities from ANAC, CVD, RD and COPD due to O_3 can increase by 87 (4.1%), 22 (4.1%), 8 (4.4%) and 7 (4.0%), respectively. In summary, affected by urban expansion and anthropogenic emissions, changes in total premature mortalities due to $PM_{2.5}$ are –6.9% and 16.0%, due to O_3 are 9.5% and 4.1%. The effects of urban expansion on health risks are in the same order (1/2 to 2 times) as those induced by anthropogenic emissions.

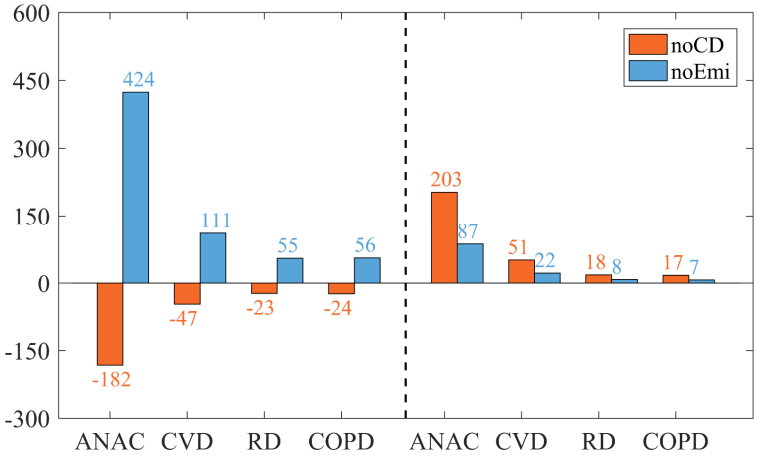

Figure 12. Differences in premature mortality from ANAC, CVD, RD and COPD attributed to $PM_{2.5}$ (left of dotted line) and O_3 (right of dotted line) exposure between baseline and sensitivity simulations. The red bars are the differences between Jan_Base and Jan_noCD simulations (Jan_Base minus Jan_noCD), and the differences between July_Base and July_noCD simulations (July_Base minus July_noCD). The blue bars are the differences between Jan_Base and Jan_noEmi simulations (Jan_Base minus Jan_noEmi), and the differences between July_Base and July_noEmi simulations (July_Base minus July_noEmi).

4 Conclusions

With the development in urbanization, urban land use and anthropogenic emissions increase, which affects urban air quality and then health risks of air pollutants. In this study, the impacts of

https://doi.org/10.5194/egusphere-2022-486
Preprint. Discussion started: 4 July 2022

urbanization on air quality and the corresponding health risks in Chengdu, a highly urbanized city with severe air pollution and complex terrain, are quantified. Management of urban air pollution is usually achieved by reducing anthropogenic emissions. So the impacts of urban expansion are further compared with anthropogenic emissions on health risks.

Chengdu is suffering from severe $PM_{2.5}$ and O_3 pollution in recent years. There are 97, 101, 68, 53, 33, 43 and 37 $PM_{2.5}$ pollution episodes, and 61, 48, 42, 40, 26, 50 and 27 O_3 pollution episodes in Chengdu from 2015 to 2021. Severe $PM_{2.5}$ and O_3 pollution pose huge health risks. The annual premature mortalities from ANAC, CVD, RD and COPD due to $PM_{2.5}$ are 9386, 2609, 1321 and 1485, due to O_3 are 7743, 1981, 648 and 630. $PM_{2.5}$ and O_3 pollution have different seasonal preferences. Due to the secondary circulation driven by complex terrain and the frequent temperature inversion, $PM_{2.5}$ pollution tends to appear in cold months (November to February). While O_3 pollution is likely to occur in warm months (April to August) because of high temperature and strong sunlight dominated by high-pressure systems. $PM_{2.5}$ has a diurnal variation with high concentrations at night but low concentrations at noon affected by the boundary layer height. O_3 exhibits strong diurnal variation with an afternoon maximum and an early morning minimum, which is related to photochemical reactions during the daytime and nitrogen oxide titration at night.

The urban land use of Chengdu is replaced by cropland in the WRF-Chem model to examine the impacts of urban expansion. Urban expansion leads to an increase in air temperature and boundary layer height, and decreases surface $PM_{2.5}$ concentrations by 11.7 μg m^{-3} in January 2017. As for O_3, the surface concentration increases by 4.4 μg m^{-3} at noon due to stronger photochemical reactions and better vertical mixing, and increases by 25.8 μg m^{-3} at midnight since the NO_x titration is weakened. MDA8 O_3 finally increases by 10.6 μg m^{-3} in July 2017 when urban land use is taken into account. In this case, the premature mortalities from ANAC, CVD, RD and COPD attributed to $PM_{2.5}$ exposure decrease by 182 (6.9%), 47 (6.5%), 23 (6.4%) and 24 (6.1%), attributed to O_3 exposure increase by 203 (9.1%), 51 (9.4%), 18 (10.0%) and 17 (9.7%). Anthropogenic emissions increase surface $PM_{2.5}$ significantly with monthly average concentration increasing by 26.6 μg m^{-3}, more than twice the difference caused by urban expansion. Due to the non-linear sensitivity of O_3 to its precursors, O_3 concentrations increase during the daytime but decrease at night. In particular, O_3 concentrations increase by 5.8 μg m^{-3} at 14:00 LST but decrease by 3.4 μg m^{-3} at 2:00 LST with anthropogenic emissions in Chengdu. Since O_3 concentrations in daytime are much higher than

https://doi.org/10.5194/egusphere-2022-486
Preprint. Discussion started: 4 July 2022

those at night, MDA8 O_3 concentrations still increase by 4.8 μg m^{-3}. As a consequence, the premature mortalities from ANAC, CVD, RD and COPD attributed to $PM_{2.5}$ exposure increase by 424 (16.0%), 111 (15.4%), 55 (15.2%) and 56 (14.3%), attributed to O_3 exposure increase by 87 (4.1%), 22 (4.1%), 8 (4.4%) and 7 (4.0%).

Our results show that the impacts of urban expansion are in the same order (1/2 to 2 times) as those induced by emissions growth on air pollutants. Although the focus of air quality management is traditionally to regulate emissions, urban planning is an ancillary option and should also be considered in future air pollution strategies.

Data Availability Statement.

Air quality monitoring data are acquired from the official NEMC real-time publishing platform (http://106.37.208.233:20035/). Meteorological data are taken from the website of the University of Wyoming (http://weather.uwyo.edu/). The NCEP global final analysis data were taken from the NCEP (https://doi.org/10.5065/D6M043C6/). The MEIC data are accessible at http://meicmodel.org/. These data can be downloaded for free as long as you agree to the official instructions.

Author contributions.

CZ and MX had the original ideas, designed the research, collected the data and prepared the original draft. CZ did the numerical simulations and carried out the data analysis. MX acquired financial support for the project leading to this publication. HL, BL and ZW collected the data. TW, BZ, ML and SL reviewed the initial draft and checked the language of the original draft.

Competing interests.

The contact author has declared that neither they nor their co-authors have any competing interests.

Acknowledgements.

We are grateful to NEMC for the air quality monitoring data, to NCDC for the meteorological data, to NCEP for global final analysis fields and to Tsinghua University for the MEIC inventories. The numerical calculations were performed on the Blade cluster system in the High Performance

https://doi.org/10.5194/egusphere-2022-486
Preprint. Discussion started: 4 July 2022

Computing and Massive Data Center (HPC&MDC) of School of Atmospheric Sciences, Nanjing University.

Financial support.

This work was supported by the open research fund of Chongqing Meteorological Bureau (KFJJ-201607), the Natural Science Foundation of Chongqing (cstc2021jcyj-msxmX1007), the Chongqing Science and Technology Commission technology innovation and application demonstration project (cstc2018jszx-zdyfxmX0003) and Innovation Team Fund of Southwest Regional Meteorological Center, China Meteorological Administration.

References

Aneja, V. P., Mathur, R., Arya, S. P., Li, Y. X., Murray, G. C., and Manuszak, T. L.: Coupling the vertical distribution of ozone in the atmospheric boundary layer, Environ. Sci. Technol., 34, 2324-2329, https://doi.org/10.1021/es990997+, 2000.

Anenberg, S. C., Horowitz, L. W., Tong, D. Q., and West, J. J.: An estimate of the global burden of anthropogenic ozone and fine particulate matter on premature human mortality using atmospheric modeling, Environ Health Perspect, 118, 1189-1195, https://doi.org/10.1289/ehp.0901220, 2010.

Baasandorj, M., Hoch, S. W., Bares, R., Lin, J. C., Brown, S. S., Millet, D. B., Martin, R., Kelly, K., Zarzana, K. J., Whiteman, C. D., Dube, W. P., Tonnesen, G., Jaramillo, I. C., and Sohl, J.: Coupling between Chemical and Meteorological Processes under Persistent Cold-Air Pool Conditions: Evolution of Wintertime $PM_{2.5}$ Pollution Events and N_2O_5 Observations in Utah's Salt Lake Valley, Environ Sci Technol, 51, 5941-5950, https://doi.org/10.1021/acs.est.6b06603, 2017.

Bahreini, R., Ahmadov, R., McKeen, S. A., Vu, K. T., Dingle, J. H., Apel, E. C., Blake, D. R., Blake, N., Campos, T. L., Cantrell, C., Flocke, F., Fried, A., Gilman, J. B., Hills, A. J., Hornbrook, R. S., Huey, G., Kaser, L., Lerner, B. M., Mauldin, R. L., Meinardi, S., Montzka, D. D., Richter, D., Schroeder, J. R., Stell, M., Tanner, D., Walega, J., Weibring, P., and Weinheimer, A.: Sources and characteristics of summertime organic aerosol in the Colorado Front Range: perspective from measurements and WRF-Chem modeling, Atmos. Chem. Phys., 18, 8293-

https://doi.org/10.5194/egusphere-2022-486
Preprint. Discussion started: 4 July 2022

8312, https://doi.org/10.5194/acp-18-8293-2018, 2018.

Baklanov, A., Molina, L. T., and Gauss, M.: Megacities, air quality and climate, Atmospheric Environment, 126, 235-249, https://doi.org/10.1016/j.atmosenv.2015.11.059, 2016.

Brauer, M., Freedman, G., Frostad, J., van Donkelaar, A., Martin, R. V., Dentener, F., van Dingenen, R., Estep, K., Amini, H., Apte, J. S., Balakrishnan, K., Barregard, L., Broday, D., Feigin, V., Ghosh, S., Hopke, P. K., Knibbs, L. D., Kokubo, Y., Liu, Y., Ma, S. F., Morawska, L., Sangrador, J. L. T., Shaddick, G., Anderson, H. R., Vos, T., Forouzanfar, M. H., Burnett, R. T., and Cohen, A.: Ambient Air Pollution Exposure Estimation for the Global Burden of Disease 2013, Environ. Sci. Technol., 50, 79-88, https://doi.org/10.1021/acs.est.5b03709, 2016.

Chen, S. H. and Sun, W. Y.: A one-dimensional time dependent cloud model, J. Meteorol. Soc. Jpn., 80, 99-118, https://doi.org/10.2151/jmsj.80.99, 2002.

Chen, R., Yin, P., Meng, X., Liu, C., Wang, L., Xu, X., Ross, J. A., Tse, L. A., Zhao, Z., Kan, H., and Zhou, M.: Fine Particulate Air Pollution and Daily Mortality. A Nationwide Analysis in 272 Chinese Cities, Am J Respir Crit Care Med, 196, 73-81, https://doi.org/10.1164/rccm.201609-1862OC, 2017.

Crosman, E. T. and Horel, J. D.: Sea and Lake Breezes: A Review of Numerical Studies, Boundary-Layer Meteorology, 137, 1-29, https://doi.org/10.1007/s10546-010-9517-9, 2010.

Dai, X. A., Johnson, B. A., Luo, P. L., Yang, K., Dong, L. X., Wang, Q., Liu, C., Li, N. W., Lu, H., Ma, L., Yang, Z. L., and Yao, Y. Z.: Estimation of Urban Ecosystem Services Value: A Case Study of Chengdu, Southwestern China, Remote Sens., 13, 24, https://doi.org/10.3390/rs13020207, 2021.

De Wekker S F J, Snyder B J. Mountain weather research and forecasting: recent progress and current challenges [M]. New York: Springer, 2013.

Fast, J. D., Gustafson, W. I., Easter, R. C., Zaveri, R. A., Barnard, J. C., Chapman, E. G., Grell, G. A., and Peckham, S. E.: Evolution of ozone, particulates, and aerosol direct radiative forcing in the vicinity of Houston using a fully coupled meteorology-chemistry-aerosol model, J. Geophys. Res.-Atmos., 111, 29, https://doi.org/10.1029/2005jd006721, 2006.

Grell, G. A. and Devenyi, D.: A generalized approach to parameterizing convection combining ensemble and data assimilation techniques, Geophys. Res. Lett., 29, 4, https://doi.org/10.1029/2002gl015311, 2002.

https://doi.org/10.5194/egusphere-2022-486
Preprint. Discussion started: 4 July 2022

554 Grell, G. A., Peckham, S. E., Schmitz, R., McKeen, S. A., Frost, G., Skamarock, W. C., and Eder,
555 B.: Fully coupled “online” chemistry within the WRF model, Atmospheric Environment, 39,
556 6957-6975, https://doi.org/10.1016/j.atmosenv.2005.04.027, 2005.
557 Guenther, A., Karl, T., Harley, P., Wiedinmyer, C., Palmer, P. I., and Geron, C.: Estimates of global
558 terrestrial isoprene emissions using MEGAN (Model of Emissions of Gases and Aerosols from
559 Nature), Atmos. Chem. Phys., 6, 3181-3210, https://doi.org/10.5194/acp-6-3181-2006, 2006.
560 Guo, H., Ling, Z. H., Cheung, K., Jiang, F., Wang, D. W., Simpson, I. J., Barletta, B., Meinardi, S.,
561 Wang, T. J., Wang, X. M., Saunders, S. M., and Blake, D. R.: Characterization of
562 photochemical pollution at different elevations in mountainous areas in Hong Kong, Atmos.
563 Chem. Phys., 13, 3881-3898, https://doi.org/10.5194/acp-13-3881-2013, 2013.
564 Holman, C., Harrison, R. M., and Querol, X.: Review of the efficacy of low emission zones to
565 improve urban air quality in European cities, Atmospheric Environment, 111, 161-169,
566 https://doi.org/10.1016/j.atmosenv.2015.04.009, 2015.
567 Hu, Y. and Wang, S.: Formation mechanism of a severe air pollution event: A case study in the
568 Sichuan Basin, Southwest China, Atmospheric Environment, 246,
569 https://doi.org/10.1016/j.atmosenv.2020.118135, 2021.
570 Hu, J., Li, Y. C., Zhao, T. L., Liu, J., Hu, X. M., Liu, D. Y., Jiang, Y. C., Xu, J. M., and Chang, L. Y.:
571 An important mechanism of regional O-3 transport for summer smog over the Yangtze River
572 Delta in eastern China, Atmos. Chem. Phys., 18, 16239-16251, https://doi.org/10.5194/acp-18-
573 16239-2018, 2018.
574 Janjic, Z. I.: THE STEP-MOUNTAIN ETA COORDINATE MODEL - FURTHER
575 DEVELOPMENTS OF THE CONVECTION, VISCOUS SUBLAYER, AND
576 TURBULENCE CLOSURE SCHEMES, Mon. Weather Rev., 122, 927-945,
577 https://doi.org/10.1175/1520-0493(1994)122<0927:Tsmecm>2.0.Co;2, 1994.
578 Jimenez, P. A. and Dudhia, J.: Improving the Representation of Resolved and Unresolved
579 Topographic Effects on Surface Wind in the WRF Model, J. Appl. Meteorol. Climatol., 51,
580 300-316, https://doi.org/10.1175/jamc-d-11-084.1, 2012.
581 Jin, X. M., Fiore, A., Boersma, K. F., De Smedt, I., and Valin, L.: Inferring Changes in Summertime
582 Surface Ozone-NOx-VOC Chemistry over US Urban Areas from Two Decades of Satellite and
583 Ground-Based Observations, Environ. Sci. Technol., 54, 6518-6529,

https://doi.org/10.5194/egusphere-2022-486
Preprint. Discussion started: 4 July 2022

https://doi.org/10.1021/acs.est.9b07785, 2020.

Karl, T., Gohm, A., Rotach, M. W., Ward, H. C., Graus, M., Cede, A., Wohlfahrt, G., Hammerle, A., Haid, M., Tiefengraber, M., Lamprecht, C., Vergeiner, J., Kreuter, A., Wagner, J., and Staudinger, M.: Studying Urban Climate and Air Quality in the Alps: The Innsbruck Atmospheric Observatory, Bull. Amer. Meteorol. Soc., 101, E488-E507, https://doi.org/10.1175/bams-d-19-0270.1, 2019.

Kinney, P. L.: Interactions of Climate Change, Air Pollution, and Human Health, Curr. Environ. Health Rep., 5, 179-186, https://doi.org/10.1007/s40572-018-0188-x, 2018.

Lee, C. S. L., Chou, C. C., Cheung, H. C., Tsai, C. Y., Huang, W. R., Huang, S. H., Chen, M. J., Liao, H. T., Wu, C. F., Tsao, T. M., Tsai, M. J., and Su, T. C.: Seasonal variation of chemical characteristics of fine particulate matter at a high-elevation subtropical forest in East Asia, Environ Pollut, 246, 668-677, https://doi.org/10.1016/j.envpol.2018.11.033, 2019.

Lelieveld, J., Barlas, C., Giannadaki, D., and Pozzer, A.: Model calculated global, regional and megacity premature mortality due to air pollution, Atmos. Chem. Phys., 13, 7023-7037, https://doi.org/10.5194/acp-13-7023-2013, 2013.

Liao, J., Wang, T., Jiang, Z., Zhuang, B., Xie, M., Yin, C., Wang, X., Zhu, J., Fu, Y., and Zhang, Y.: WRF/Chem modeling of the impacts of urban expansion on regional climate and air pollutants in Yangtze River Delta, China, Atmospheric Environment, 106, 204-214, https://doi.org/10.1016/j.atmosenv.2015.01.059, 2015.

Lin, B. and Zhu, J.: Changes in urban air quality during urbanization in China, J. Clean Prod., 188, 312-321, https://doi.org/10.1016/j.jclepro.2018.03.293, 2018.

Liu, H., Liu, S., Xue, B., Lv, Z., Meng, Z., Yang, X., Xue, T., Yu, Q., and He, K.: Ground-level ozone pollution and its health impacts in China, Atmospheric Environment, 173, 223-230, https://doi.org/10.1016/j.atmosenv.2017.11.014, 2018.

Lu, H. X., Lyu, X. P., Cheng, H. R., Ling, Z. H., and Guo, H.: Overview on the spatial-temporal characteristics of the ozone formation regime in China, Environ. Sci.-Process Impacts, 21, 916-929, https://doi.org/10.1039/c9em00098d, 2019.

Luo, Y. L., Shen, J., Chen, A. F., Tao, Q., Li, Q. Q., White, P. J., Li, T. Q., Li, B., Chen, L., Li, H. X., Gao, X. S., Xu, Q., and Wang, C. Q.: Loss of organic carbon in suburban soil upon urbanization of Chengdu megacity, China, Sci. Total Environ., 785, 10,

https://doi.org/10.5194/egusphere-2022-486
Preprint. Discussion started: 4 July 2022

https://doi.org/10.1016/j.scitotenv.2021.147209, 2021.

Manisalidis, I., Stavropoulou, E., Stavropoulos, A., and Bezirtzoglou, E.: Environmental and Health Impacts of Air Pollution: A Review, Frontiers in Public Health, 8, https://doi.org/10.3389/fpubh.2020.00014, 2020.

Matsui, T., Zhang, S. Q., Lang, S. E., Tao, W. K., Ichoku, C., and Peters-Lidard, C. D.: Impact of radiation frequency, precipitation radiative forcing, and radiation column aggregation on convection-permitting West African monsoon simulations, Clim. Dyn., 55, 193-213, https://doi.org/10.1007/s00382-018-4187-2, 2018.

Mlawer, E. J., Taubman, S. J., Brown, P. D., Iacono, M. J., and Clough, S. A.: Radiative transfer for inhomogeneous atmospheres: RRTM, a validated correlated-k model for the longwave, J. Geophys. Res.-Atmos., 102, 16663-16682, https://doi.org/10.1029/97jd00237, 1997.

Molina, L. T., Madronich, S., Gaffney, J. S., Apel, E., de Foy, B., Fast, J., Ferrare, R., Herndon, S., Jimenez, J. L., Lamb, B., Osornio-Vargas, A. R., Russell, P., Schauer, J. J., Stevens, P. S., Volkamer, R., and Zavala, M.: An overview of the MILAGRO 2006 Campaign: Mexico City emissions and their transport and transformation, Atmos. Chem. Phys., 10, 8697-8760, https://doi.org/10.5194/acp-10-8697-2010, 2010.

Ning, G., Wang, S., Yim, S. H. L., Li, J., Hu, Y., Shang, Z., Wang, J., and Wang, J.: Impact of low-pressure systems on winter heavy air pollution in the northwest Sichuan Basin, China, Atmos. Chem. Phys., 18, 13601-13615, https://doi.org/10.5194/acp-18-13601-2018, 2018.

Oke, T. R.; Mills, G.; Christen, A.; Voogt, J. A. Urban Climates; Cambridge University Press: Cambridge, 2017.

Pautasso, M., Dehnen-Schmutz, K., Holdenrieder, O., Pietravalle, S., Salama, N., Jeger, M. J., Lange, E., and Hehl-Lange, S.: Plant health and global change - some implications for landscape management, Biol. Rev., 85, 729-755, https://doi.org/10.1111/j.1469-185X.2010.00123.x, 2010.

Qian, Y., Chakraborty, T. C., Li, J., Li, D., He, C., Sarangi, C., Chen, F., Yang, X., and Leung, L. R.: Urbanization Impact on Regional Climate and Extreme Weather: Current Understanding, Uncertainties, and Future Research Directions, Adv Atmos Sci, 1-42, https://doi.org/10.1007/s00376-021-1371-9, 2022.

Ryu, Y. H., Baik, J. J., Kwak, K. H., Kim, S., and Moon, N.: Impacts of urban land-surface forcing

https://doi.org/10.5194/egusphere-2022-486
Preprint. Discussion started: 4 July 2022

on ozone air quality in the Seoul metropolitan area, Atmos. Chem. Phys., 13, 2177-2194, https://doi.org/10.5194/acp-13-2177-2013, 2013.

Schell, B., Ackermann, I. J., Hass, H., Binkowski, F. S., and Ebel, A.: Modeling the formation of secondary organic aerosol within a comprehensive air quality model system, J. Geophys. Res.-Atmos., 106, 28275-28293, https://doi.org/10.1029/2001jd000384, 2001.

Seto, K. C., Guneralp, B., and Hutyra, L. R.: Global forecasts of urban expansion to 2030 and direct impacts on biodiversity and carbon pools, Proc. Natl. Acad. Sci. U. S. A., 109, 16083-16088, https://doi.org/10.1073/pnas.1211658109, 2012.

Shu, Z., Liu, Y., Zhao, T., Xia, J., Wang, C., Cao, L., Wang, H., Zhang, L., Zheng, Y., Shen, L., Luo, L., and Li, Y.: Elevated 3D structures of $PM_{2.5}$ and impact of complex terrain-forcing circulations on heavy haze pollution over Sichuan Basin, China, Atmos. Chem. Phys., 21, 9253-9268, https://doi.org/10.5194/acp-21-9253-2021, 2021.

Song, Y., Wang, X., Maher, B. A., Li, F., Xu, C., Liu, X., Sun, X., and Zhang, Z.: The spatial-temporal characteristics and health impacts of ambient fine particulate matter in China, J. Clean Prod., 112, 1312-1318, https://doi.org/10.1016/j.jclepro.2015.05.006, 2015.

Stockwell, W. R., Middleton, P., Chang, J. S., and Tang, X. Y.: THE 2ND GENERATION REGIONAL ACID DEPOSITION MODEL CHEMICAL MECHANISM FOR REGIONAL AIR-QUALITY MODELING, J. Geophys. Res.-Atmos., 95, 16343-16367, https://doi.org/10.1029/JD095iD10p16343, 1990.

Tang, G. Q., Zhu, X. W., Xin, J. Y., Hu, B., Song, T., Sun, Y., Zhang, J. Q., Wang, L. L., Cheng, M. T., Chao, N., Kong, L. B., Li, X., and Wang, Y. S.: Modelling study of boundary-layer ozone over northern China - Part I: Ozone budget in summer, Atmos. Res., 187, 128-137, https://doi.org/10.1016/j.atmosres.2016.10.017, 2017.

Tewari, M., Chen, F., Wang, W., Dudhia, J., LeMone, M., Mitchell, K., Ek, M., Gayno, G., Wegiel, J., and Cuenca, R.: Implementation and verification of the unified NOAH land surface model in the WRF model, 20th conference on weather analysis and forecasting/16th conference on numerical weather prediction, 2165-2170.

UN DESA, 2018: World Urbanization Prospects: The 2018 Revision. United Nations Department of Economic and Social Affairs, Population Division.

Wang, P., Shen, J., Xia, M., Sun, S., Zhang, Y., Zhang, H., and Wang, X.: Unexpected enhancement

https://doi.org/10.5194/egusphere-2022-486
Preprint. Discussion started: 4 July 2022

of ozone exposure and health risks during National Day in China, Atmos. Chem. Phys., 21, 10347-10356, https://doi.org/10.5194/acp-21-10347-2021, 2021.

Whiteman C D. Mountain meteorology: fundamentals and applications [M]. Oxford University Press, 2000.

Yang, X., Wu, K., Wang, H., Liu, Y., Gu, S., Lu, Y., Zhang, X., Hu, Y., Ou, Y., Wang, S., and Wang, Z.: Summertime ozone pollution in Sichuan Basin, China: Meteorological conditions, sources and process analysis, Atmospheric Environment, 226, https://doi.org/10.1016/j.atmosenv.2020.117392, 2020.

Yin, P., Chen, R., Wang, L., Meng, X., Liu, C., Niu, Y., Lin, Z., Liu, Y., Liu, J., Qi, J., You, J., Zhou, M., and Kan, H.: Ambient Ozone Pollution and Daily Mortality: A Nationwide Study in 272 Chinese Cities, Environ Health Perspect, 125, 117006, https://doi.org/10.1289/EHP1849, 2017.

Zhan, C. and Xie, M.: Land use and anthropogenic heat modulate ozone by meteorology: a perspective from the Yangtze River Delta region, Atmos. Chem. Phys., 22, 1351-1371, https://doi.org/10.5194/acp-22-1351-2022, 2022.

Zhan, C., Xie, M., Liu, J., Wang, T., Xu, M., Chen, B., Li, S., Zhuang, B., and Li, M.: Surface Ozone in the Yangtze River Delta, China: A Synthesis of Basic Features, Meteorological Driving Factors, and Health Impacts, Journal of Geophysical Research: Atmospheres, 126, https://doi.org/10.1029/2020jd033600, 2021.

Zhan, C.-c., Xie, M., Fang, D.-x., Wang, T.-j., Wu, Z., Lu, H., Li, M.-m., Chen, P.-l., Zhuang, B.-l., Li, S., Zhang, Z.-q., Gao, D., Ren, J.-y., and Zhao, M.: Synoptic weather patterns and their impacts on regional particle pollution in the city cluster of the Sichuan Basin, China, Atmospheric Environment, 208, 34-47, https://doi.org/10.1016/j.atmosenv.2019.03.033, 2019.

Zhu, K. G., Xie, M., Wang, T. J., Cai, J. X., Li, S. B., and Feng, W.: A modeling study on the effect of urban land surface forcing to regional meteorology and air quality over South China, Atmospheric Environment, 152, 389-404, https://doi.org/10.1016/j.atmosenv.2016.12.053, 2017.